COMPUTATIONAL METHODS FOR 2D SHALLOW WATER FLOWS BASED ON RELAXATION SCHEMES

A. I. DELIS and Th. KATSAOUNIS
Department of Applied Mathematics, University of Crete, Heraklion 71409, Crete, Greece
and
Institute of Applied and Computational Mathematics, FORTH, Heraklion 71110, Crete, Greece
Email: adelis@tem.uoc.gr and thodoros@tem.uoc.gr

***Abstract*— Computational models for the solution of the two-dimensional shallow water equations (SWEs) are presented. We describe a generalized class of first and second order in space and time relaxation schemes for the SWEs in two dimensions. We extend in 2D classical relaxation models combined with Runge-Kutta time stepping mechanisms as to include also a forcing source term. To illustrate and validate the capabilities of the proposed models, results are presented for various well known test problems with or without the source term present.**

I. Introduction

The mathematical model used here consists of the 2D SWEs, in their classical form, obtained from the incompressible flow continuity equation and the momentum balance Navier-Stokes equations, written in its physical conservative form as a single vector equation

$$\mathbf{U}_t+\mathbf{F}(\mathbf{U})_x+\mathbf{G}(\mathbf{U})_y = \mathbf{S}(\mathbf{U}), \quad (x,y)\in\Omega, \quad (1)$$

where

$$\mathbf{U} = \left(\ h, hu_1, hu_2 \ \right)^{\mathrm{T}} = \left(\ h, q_1, q_2, \ \right)^{\mathrm{T}},$$

$$\mathbf{S}(\mathbf{U}) = \left(\ 0, -gh\frac{\partial Z}{\partial x}(x,y), -gh\frac{\partial Z}{\partial y}(x,y), \ \right)^{\mathrm{T}},$$

$$\mathbf{F}(\mathbf{U}) = \left(\ q_1, \frac{q_1^2}{h}+\frac{1}{2}gh^2, \frac{q_1 q_2}{h} \ \right)^{\mathrm{T}},$$

$$\mathbf{G}(\mathbf{U}) = \left(\ q_2, \frac{q_1 q_2}{h}, \frac{q_2^2}{h}+\frac{1}{2}gh^2 \ \right)^{\mathrm{T}}.$$

System (1) describes the flow at time $t \geq 0$ at point $(x,y) \in \Omega$, where $h(x,y,t) \geq 0$ is the height of the fluid at point (x,y) at time t, Ω denotes the projection of the domain occupied by the fluid onto the xy plane and $Z(x,y)$ is the bottom height function. The vector field (u_1,u_2) is the average horizontal velocity, and g the gravitational acceleration. Finally, the conservative variable q (discharge) is given by $(q_1,q_2) = (hu_1,hu_2)$. In the homogeneous case, the system is equivalent to that of isentropic Euler system. However due to the presence of the source term the properties of the system change substantially. The above system is quite simple in the sense that only the topography of the bottom in taken into account, but other terms could be also added in order to include effects such as friction on the bottom and on the surface as well as variations of the channel width.

Substantial effort has been devoted over the past 20 years to the development of computational techniques for fluid flow simulation, in particular in the field of finite volumes for systems of conservation laws. More recently many methods were proposed for the numerical approximation of solutions of hyperbolic conservations laws with source terms. There has been a growing trend in favor of Riemann

or Godunov-type based methods constructed within the finite volume framework, see for example [11]. Such methods are noted for their good conservation and shock capturing capabilities. Two dimensional Riemann solvers do not appear to have matured enough to be used in the construction of multi-dimensional schemes. Even if such solvers were available the resulting schemes are likely to be too complicated for common use. The purpose of the present work is to report on the applicability of recently developed relaxation algorithms for shallow flows, introduced in [4] in one-dimension, for computing solutions in two-dimensions. We use finite volume shock capturing spatial discretizations that are Riemann solver free, while a Runge–Kutta method provides the time stepping mechanisms. The proposed schemes combine simplicity and high efficiency. Their performance in various test problems shows that provide a reliable alternative for shallow water wave computations in one and two dimensions. Numerical results are presented for several test problems with or without the source term present. The presented schemes are verified by comparing the results with documented ones.

II. Relaxation systems for the 2D SWEs

Relaxation systems for the 2D SWEs are motivated by the general relaxation systems presented in [6] and the relaxation systems introduced in [4] for the 1D SWEs. Following from the above we write a relaxation system for the SWEs replacing the conservation law (1) by a larger linear system, setting

$$\mathbf{u} = \begin{bmatrix} h, \\ q_1, \\ q_2 \end{bmatrix}, \quad \mathbf{v} = \begin{bmatrix} v_1, \\ v_2, \\ v_3 \end{bmatrix}, \quad \mathbf{w} = \begin{bmatrix} w_1, \\ w_2, \\ w_3 \end{bmatrix},$$

system (1) can be written as

$$\begin{aligned} \mathbf{u}_t + \mathbf{v}_x + \mathbf{w}_y &= \mathbf{S}(\mathbf{u}), \\ \mathbf{v}_t + \mathbf{C}^2\mathbf{u}_x &= -\frac{1}{\epsilon}(\mathbf{v} - \mathbf{F}(\mathbf{u})) \\ \mathbf{w}_t + \mathbf{D}^2\mathbf{u}_y &= -\frac{1}{\epsilon}(\mathbf{w} - \mathbf{G}(\mathbf{u})), \end{aligned} \tag{2}$$

where $\mathbf{C}^2, \mathbf{D}^2 \in \mathbb{R}^{3\times 3}$ are positive diagonal matrices, e.g. $\mathbf{C}^2 = diag(c_1^2, c_2^2, c_3^2)$. System (2) can now be further reformulated as,

$$\begin{aligned} &\begin{bmatrix} \mathbf{u} \\ \mathbf{v} \\ \mathbf{w} \end{bmatrix}_t + \begin{bmatrix} 0 & \mathbf{I} & 0 \\ \mathbf{C}^2 & 0 & 0 \\ 0 & 0 & 0 \end{bmatrix} \begin{bmatrix} \mathbf{u} \\ \mathbf{v} \\ \mathbf{w} \end{bmatrix}_x \\ &\quad + \begin{bmatrix} 0 & 0 & \mathbf{I} \\ 0 & 0 & 0 \\ \mathbf{D}^2 & 0 & 0 \end{bmatrix} \begin{bmatrix} \mathbf{u} \\ \mathbf{v} \\ \mathbf{w} \end{bmatrix}_y = \\ &\quad = \begin{bmatrix} \mathbf{S}(\mathbf{u}) \\ -\frac{1}{\epsilon}(\mathbf{v} - \mathbf{F}(\mathbf{u})) \\ -\frac{1}{\epsilon}(\mathbf{w} - \mathbf{G}(\mathbf{u})) \end{bmatrix}. \end{aligned} \tag{3a}$$

We also consider the following variant, of the above relaxation system, based on a novel approach presented in [4] for the 1D case, written in vector form as

$$\begin{aligned} &\begin{bmatrix} \mathbf{u} \\ \mathbf{v} \\ \mathbf{w} \end{bmatrix}_t + \begin{bmatrix} 0 & \mathbf{I} & 0 \\ \mathbf{C}^2 & 0 & 0 \\ 0 & 0 & 0 \end{bmatrix} \begin{bmatrix} \mathbf{u} \\ \mathbf{v} \\ \mathbf{w} \end{bmatrix}_x \\ &\quad + \begin{bmatrix} 0 & 0 & \mathbf{I} \\ 0 & 0 & 0 \\ \mathbf{D}^2 & 0 & 0 \end{bmatrix} \begin{bmatrix} \mathbf{u} \\ \mathbf{v} \\ \mathbf{w} \end{bmatrix}_y = \\ &\quad = \begin{bmatrix} 0 \\ -\frac{1}{\epsilon}(\mathbf{v} - \mathbf{F}(\mathbf{u})) - \frac{1}{\epsilon}\widetilde{\mathbf{S}}(\mathbf{u}) \\ -\frac{1}{\epsilon}(\mathbf{w} - \mathbf{G}(\mathbf{u})) - \frac{1}{\epsilon}\widetilde{\widetilde{\mathbf{S}}}(\mathbf{u}) \end{bmatrix}. \end{aligned} \tag{3b}$$

where

$$\widetilde{\mathbf{S}}(\mathbf{u}) = \begin{bmatrix} 0 \\ -\int^x gh(s,y)\frac{\partial Z}{\partial x}(s,y)ds \\ 0 \end{bmatrix}$$

and

$$\tilde{\tilde{\mathbf{S}}}(\mathbf{u}) = \begin{bmatrix} 0 \\ 0 \\ -\int^y gh(x,s)\frac{\partial Z}{\partial y}(x,s)ds \end{bmatrix}.$$

The original conservation law, in both formulations, has now been replaced by a linear hyperbolic system with a relaxation source term which rapidly drives $\mathbf{v} \to \mathbf{F}(\mathbf{u})$ and $\mathbf{w} \to \mathbf{G}(\mathbf{u})$ in the relaxation limit $\epsilon \to 0$. In some cases it can be shown analytically that solutions of the linear system approach solutions to the original conservation law.

A general necessary condition for such convergence is that the *subcharacteristic condition* is satisfied. For systems (3) we require that for the eigenvalues λ_i of $\mathbf{F}'(\mathbf{u})$ and eigenvalues μ_i of $\mathbf{G}'(\mathbf{u})$ the following condition to be satisfied

$$\frac{\lambda_1}{c_1} + \frac{\lambda_2}{c_2} + \frac{\lambda_3}{c_3} + \frac{\mu_1}{d_1} + \frac{\mu_2}{d_2} + \frac{\mu_3}{d_3} \leq 1. \quad (4)$$

By doing so we insure that the characteristic speeds of the hyperbolic part of (3a) or (3b) are at least as large as the characteristic speeds of the original problem. Hence, by choosing the constants c_1, c_2, c_3 and d_1, d_2, d_3, appropriately, so that the corresponding subcharacteristic condition hold true, in the relaxation limit $\epsilon \to 0$ we recover (1), for both relaxation systems (3a) and (3b). See for example, [9], [10], [8], [7] for discussions of this condition and convergence properties.

III. Semi-discrete relaxation schemes

We consider the classical second order MUSCL-TVD scheme for the spatial discretization. For brevity we present the semi-discrete schemes for system (3b). To discretize the system of equations, a spatially 2D domain of integration, divided into cells (i,j), is assumed, with a uniform grid widths in each direction, $\Delta x = x_{i+\frac{1}{2}} - x_{i-\frac{1}{2}}$, $\Delta y = y_{i+\frac{1}{2}} - y_{i-\frac{1}{2}}$ and time step $\Delta t = t^{n+1} - t^n, \quad n = 0, 1, 2, \ldots$. The approximate solution, denoted as the discrete value $\mathbf{u}_{ij}^n$, is the approximate cell average of the variable $\mathbf{u}$ in the cell $(x_{i+\frac{1}{2}}, x_{i-\frac{1}{2}}) \times (y_{i+\frac{1}{2}}, y_{i-\frac{1}{2}})$ at time $t = t^n$. The approximate point value of $\mathbf{u}$ at $(x,y) = (x_{i+\frac{1}{2}}, y_{j+\frac{1}{2}})$ at time $t = t^n$ is denoted by $\mathbf{u}_{i+\frac{1}{2},j+\frac{1}{2}}^n$.

We start by considering the following one-step conservative system for the homogeneous case

$$\frac{\partial}{\partial t}\mathbf{u}_{ij} + \frac{1}{\Delta x}(\mathbf{v}_{i+\frac{1}{2},j} - \mathbf{v}_{i-\frac{1}{2},j}) + \frac{1}{\Delta y}(\mathbf{w}_{i,j+\frac{1}{2},} - \mathbf{w}_{i,j-\frac{1}{2}}) = 0, \quad (5a)$$

$$\frac{\partial}{\partial t}\mathbf{v}_{ij} + \frac{1}{\Delta x}\mathbf{C}^2(\mathbf{u}_{i+\frac{1}{2},j} - \mathbf{u}_{i-\frac{1}{2},j}) = -\frac{1}{\epsilon}(\mathbf{v}_{ij} - \mathbf{F}(\mathbf{u}_{ij})), \quad (5b)$$

$$\frac{\partial}{\partial t}\mathbf{w}_{ij} + \frac{1}{\Delta y}\mathbf{D}^2(\mathbf{u}_{i,j+\frac{1}{2}} - \mathbf{u}_{i,j-\frac{1}{2}}) = -\frac{1}{\epsilon}(\mathbf{w}_{ij} - \mathbf{G}(\mathbf{u}_{ij})). \quad (5c)$$

The linear hyperbolic part of the (5) has two Riemann invariants in each direction, $\mathbf{v} \pm \mathbf{C}\mathbf{u}$ in the $x-$direction and $\mathbf{w} \pm \mathbf{D}\mathbf{u}$ in the $y-$direction, associated with the characteristic fields $\pm\mathbf{C}$ and $\pm\mathbf{D}$ respectively. To construct a second order accurate in space scheme, the MUSCL piecewise linear interpolation is applied to the $k-$th component of $\mathbf{v} \pm \mathbf{C}\mathbf{u}$, which gives respectively:

$$\begin{aligned}
(v + c_k u)_{i+\frac{1}{2},j} &= (v + c_k u)_{ij} + \frac{1}{2}\Delta x s_{ij}^{x,+}, \\
(v - c_k u)_{i+\frac{1}{2},j} &= (v - c_k u)_{i+1,j} - \frac{1}{2}\Delta x s_{i+1,j}^{x,-}, \\
(w + d_k u)_{i,j+\frac{1}{2}} &= (w + d_k u)_{ij} + \frac{1}{2}\Delta y s_{ij}^{y,+}, \\
(w - d_k u)_{i,j+\frac{1}{2}} &= (v - d_k u)_{i,j+1} - \frac{1}{2}\Delta y s_{i,j+1}^{y-},
\end{aligned} \quad (6)$$

where u, v are the $k-$th ($1 \leq k \leq 3$ for the 2D SWEs) components of $\mathbf{v}, \mathbf{u}$ and $\mathbf{w}$ respectively, with s the slopes in the $(i,j)-$th cell defined as

$$s_{ij}^{x,\pm} = \frac{1}{\Delta x}(v_{i+1,j} \pm c_k u_{i+1,j} - v_{ij} \mp c_k u_{ij})\phi(\theta_{ij}^{x,\pm})$$

with

$$\theta_{ij}^{x,\pm} = \frac{v_{ij} \pm c_k u_{ij} - v_{i-1,j} \mp c_k u_{i-1,j}}{v_{i+1,j} \pm c_k u_{i+1,j} - v_{i,j} \mp c_k u_{ij}},$$

and

$$s_{ij}^{y,\pm} = \frac{1}{\Delta y}(w_{i,j+1} \pm d_k u_{i,j+1} - w_{ij} \mp d_k u_{ij})\phi(\theta_{ij}^{y,\pm})$$

with

$$\theta_{ij}^{y,\pm} = \frac{w_{ij} \pm d_k u_{ij} - v_{i,j-1} \mp d_k u_{i,j-1}}{w_{i,j+1} \pm d_k u_{i,j+1} - v_{i,j} \mp d_k u_{ij}},$$

where ϕ is a *limiter* function. There are several options on choosing a limiter function. Some of the most popular ones are, the MinMod (MM) limiter $\phi(\theta) = \max(0, \min(1, \theta))$, the Superbee (SB) limiter $\phi(\theta) = \max(0, \min(2\theta, 1), \min(\theta, 2))$, the VanLeer (VL) limiter $\phi(\theta) = \frac{|\theta|+\theta}{1+|\theta|}$, and the Monotonized Central (MC) limiter $\phi(\theta) = \max(0, \min((1+\theta)/2, 2, 2\theta))$.

Following from (6) we get

$$\begin{aligned} u_{i+\frac{1}{2},j} &= \frac{1}{2}(u_{ij} + u_{i+1,j}) - \frac{1}{2c_k}(v_{i+1,j} - v_{ij}) \\ &\quad + \frac{\Delta x}{4c_k}(s_{ij}^{x,+} + s_{i+1,j}^{x,-}), \\ v_{i+\frac{1}{2},j} &= \frac{1}{2}(v_{ij} + v_{i+1,j}) - \frac{c_k}{2}(u_{i+1,j} - u_{ij}) \\ &\quad + \frac{\Delta x}{4}(s_{ij}^{x,+} - s_{i+1,j}^{x,-}), \end{aligned} \tag{7}$$

$$\begin{aligned} u_{i,j+\frac{1}{2}} &= \frac{1}{2}(u_{ij} + u_{i,j+1}) - \frac{1}{2c_k}(w_{i,j+1} - w_{ij}) \\ &\quad + \frac{\Delta y}{4d_k}(s_{ij}^{y,+} + s_{i,j+1}^{y,-}), \\ w_{i,j+\frac{1}{2}} &= \frac{1}{2}(w_{ij} + w_{i,j+1}) - \frac{d_k}{2}(u_{i,j+1} - u_{ij}) \\ &\quad + \frac{\Delta y}{4}(s_{ij}^{y,+} - s_{i,j+1}^{y,-}). \end{aligned} \tag{8}$$

Then the second order (in space) semi-implicit relaxation scheme is given componentwise by

$$\begin{aligned} &\frac{\partial}{\partial t}u_{ij} + \frac{(v_{i+1,j} - v_{i-1,j})}{2\Delta x} \\ &\quad - \frac{c_k(u_{i+1,j} - 2u_{ij} + u_{i-1,j})}{2\Delta x} \\ &\quad - \frac{d_k(w_{i,j+1} - 2w_{ij} + w_{i,j-1})}{2\Delta y} \\ &\quad + \frac{1}{4}(s_{ij}^{x,+} - s_{i+1,j}^{x,-} - s_{i-1,j}^{x,+} + s_{ij}^{x,-}) \\ &\quad + \frac{1}{4}(s_{ij}^{y,+} - s_{i,j+1}^{y,-} - s_{i,j-1}^{y,+} + s_{ij}^{y,-}) = 0, \\ &\frac{\partial}{\partial t}v_{ij} + \frac{c_k^2(u_{i+1,j} - u_{i-1,j})}{2\Delta x} \\ &\quad - \frac{c_k(v_{i+1,j} - 2v_{ij} + v_{i-1,j})}{2\Delta x} \\ &\quad + \frac{c_k}{4}(s_{ij}^{x,+} + s_{i+1,j}^{x,-} - s_{i-1,j}^{x,+} - s_{ij}^{x,-}) = \\ &\quad - \frac{1}{\epsilon}(v_{ij} - F_k(u_{ij})) - \frac{1}{\epsilon}\widetilde{S}_k(u_{ij}), \\ &\frac{\partial}{\partial t}w_{ij} + \frac{d_k^2(u_{i,j+1} - u_{i,j-1})}{2\Delta y} \\ &\quad - \frac{d_k(w_{i,j+1} - 2w_{ij} + w_{i,j-1})}{2\Delta y} \\ &\quad + \frac{d_k}{4}(s_{ij}^{y,+} + s_{i+1,j}^{y,-} - s_{i-1,j}^{y,+} - s_{ij}^{y,-}) = \\ &\quad - \frac{1}{\epsilon}(w_{ij} - G_k(u_{ij})) - \frac{1}{\epsilon}\widetilde{\widetilde{S}}_k(u_{ij}), \end{aligned} \tag{9}$$

with $\widetilde{S}_k, \widetilde{\widetilde{S}}_k, F_k, G_k$ being the $k-$th components of $\widetilde{\mathbf{S}}, \widetilde{\widetilde{\mathbf{S}}}, \mathbf{F}$ and $\mathbf{G}$ respectively. Notice that in the case the slope $s^{\pm} = 0$ or $\phi = 0$, the MUSCL scheme (9) reduces to a first order *upwind scheme*.

IV. Fully discrete schemes

In this section we present the time discretization of the semi-discrete relaxation schemes applied to the SWEs. We apply the implicit Runge-Kutta splitting scheme introduced in [6] as the time marching mechanism to advance the solution by one time step Δt. The splitting treats, alternatively, the stiff source terms implicitly in two steps and the convection terms with two explicit steps. For the source term application, corresponding to system (3b), and temporarily dropping the subscript indices, given

$\{\mathbf{u}^n, \mathbf{v}^n\, \mathbf{w}^n\}$, then $\{\mathbf{u}^{n+1}, \mathbf{v}^{n+1}\mathbf{w}^{n+1}\}$ are computed by

$$
\begin{aligned}
\mathbf{u}^{n,1} &= \mathbf{u}^n, \\
\mathbf{v}^{n,1} &= \mathbf{v}^n + \frac{\Delta t}{\epsilon}(\mathbf{v}^{n,1} - \mathbf{F}(\mathbf{u}^{n,1})) + \frac{\Delta t}{\epsilon}\widetilde{\mathbf{S}}(\mathbf{u}^{n,1}), \\
\mathbf{w}^{n,1} &= \mathbf{w}^n + \frac{\Delta t}{\epsilon}(\mathbf{w}^{n,1} - \mathbf{G}(\mathbf{u}^{n,1})) + \frac{\Delta t}{\epsilon}\widetilde{\widetilde{\mathbf{S}}}(\mathbf{u}^{n,1}); \\
\mathbf{u}^{(1)} &= \mathbf{u}^{n,1} - \Delta t(\Delta_+^x \mathbf{v}^{n,1} + \Delta_+^y \mathbf{w}^{n,1}), \\
\mathbf{v}^{(1)} &= \mathbf{v}^{n,1} - \Delta t \mathbf{C}^2 \Delta_+^x \mathbf{u}^{n,1}, \\
\mathbf{w}^{(1)} &= \mathbf{w}^{n,1} - \Delta t \mathbf{D}^2 \Delta_+^y \mathbf{u}^{n,1}; \\
\mathbf{u}^{n,2} &= \mathbf{u}^{(1)}, \\
\mathbf{v}^{n,2} &= \mathbf{v}^{(1)} - \frac{\Delta t}{\epsilon}(\mathbf{v}^{n,2} - \mathbf{F}(\mathbf{u}^{n,2})) \\
&\quad - \frac{2\Delta t}{\epsilon}(\mathbf{v}^{n,1} - \mathbf{F}(\mathbf{u}^{n,1})) \\
&\quad - \frac{\Delta t}{\epsilon}\widetilde{\mathbf{S}}(\mathbf{u}^{n,2}) - \frac{2\Delta t}{\epsilon}\widetilde{\mathbf{S}}(\mathbf{u}^{n,1}), \\
\mathbf{w}^{n,2} &= \mathbf{w}^{(1)} - \frac{\Delta t}{\epsilon}(\mathbf{w}^{n,2} - \mathbf{G}(\mathbf{u}^{n,2})) \\
&\quad - \frac{2\Delta t}{\epsilon}(\mathbf{w}^{n,1} - \mathbf{G}(\mathbf{u}^{n,1})) \\
&\quad - \frac{\Delta t}{\epsilon}\widetilde{\widetilde{\mathbf{S}}}(\mathbf{u}^{n,2}) - \frac{2\Delta t}{\epsilon}\widetilde{\widetilde{\mathbf{S}}}(\mathbf{u}^{n,1}); \\
\mathbf{u}^{(2)} &= \mathbf{u}^{n,2} - \Delta t(\Delta_+^x \mathbf{v}^{n,2} + \Delta_+^y \mathbf{w}^{n,2}), \\
\mathbf{v}^{(2)} &= \mathbf{v}^{n,2} - \Delta t \mathbf{C}^2 \Delta_+^x \mathbf{u}^{n,2} \\
\mathbf{w}^{(2)} &= \mathbf{w}^{n,2} - \Delta t \mathbf{D}^2 \Delta_+^y \mathbf{u}^{n,2}; \\
\mathbf{u}^{n+1} &= \frac{1}{2}(\mathbf{u}^n + \mathbf{u}^{(2)}), \\
\mathbf{v}^{n+1} &= \frac{1}{2}(\mathbf{v}^n + \mathbf{v}^{(2)}), \\
\mathbf{w}^{n+1} &= \frac{1}{2}(\mathbf{w}^n + \mathbf{w}^{(2)}),
\end{aligned}
$$

where the discretization operators Δ are defined as

$$
\begin{aligned}
\Delta_+^x \mathbf{p}_{ij} &= \frac{1}{\Delta x}(\mathbf{p}_{i+\frac{1}{2},j} - \mathbf{p}_{i-\frac{1}{2},j}), \\
\Delta_+^y \mathbf{p}_{ij} &= \frac{1}{\Delta y}(\mathbf{p}_{i,j+\frac{1}{2}} - \mathbf{p}_{i,j-\frac{1}{2}}).
\end{aligned}
$$

Note that, using the above schemes neither linear algebraic equation nor nonlinear source terms arise and the space time discretizations are treated separately. In addition both first and second order relaxation schemes are stable under a *CFL* condition

$$
\max\left((\max_i c_i)\frac{\Delta t}{\Delta x}, (\max_i d_i)\frac{\Delta t}{\Delta y}\right) \leq \frac{1}{2} \qquad (12)
$$

V. Numerical tests and results

In this section we present some classical numerical tests and results that demonstrate the performance of the relaxation schemes presented for the 2D SWEs. First two typical examples of 2D dam-break problems are solved and discussed.

We choose the initial conditions for all the relaxation systems presented above as $\mathbf{u}(x,y,0) = \mathbf{u}_0(x,y)$, $\mathbf{v}(x,y,0) = \mathbf{v}_0(x,y) \equiv \mathbf{F}(\mathbf{u}_0(x,y))$, $\mathbf{w}(x,y,0) = \mathbf{w}_0(x,y) \equiv \mathbf{G}(\mathbf{u}_0(x,y))$. In the small relaxation limit ($\epsilon \to 0$) the relaxation systems presented here satisfy the so called *local equilibrium* ($\mathbf{v} = \mathbf{F}(\mathbf{u})$ and $\mathbf{w} = \mathbf{G}(\mathbf{u})$, see [6], and by choosing the above for $\mathbf{v}$ and $\mathbf{w}$ we avoid the introduction of an initial layer through the relaxation system. For the boundary conditions given the physical boundary conditions, $\mathbf{u}_b$, that should imposed for each problem (transmisive or reflective in the following test problems), then we set $\mathbf{v}_b = \mathbf{F}(\mathbf{u}_b)$ and $\mathbf{w}_b = \mathbf{G}(\mathbf{u}_b)$ as to avoid the introduction of artificial boundary layers.

The choices of $c_i, d_i, i = 1,2,3$ in all the numerical tests are based on rough estimates of the eigenvalues of the original SWEs, as to satisfy the subcharacteristic condition (4). Other choices can be made as long as numerical stability is maintained. It should be noted here that larger values for the c_i, d_i, usually add more numerical viscosity, so for accuracy reasons it is desirable to have the c_i, d_i as small as possible.

The relaxation parameter ϵ should be small with respect to the time step and space mesh length, that is $\Delta t \gg \epsilon\ \Delta y, \Delta x \gg \epsilon$. Again here, ϵ plays the role of viscosity coefficient so more numerical diffusion will be added for relatively larger values of ϵ.

A. 2D Partial Dam-Break

The first two-dimensional hypothetical problem is the one presented in [5]. For this problem a dam, located in the center of the region, is assumed to partially fail instantaneously. The water depth upstream of the dam is $h_u = 10m$ and downstream is assumed to be either $h_d = 5, 0.1, 0m$ (dry). The computational domain is a $200m \times 200m$ region which has been subdivided into 41×41 square grid. The breach is $75m$ in length, which has distances of 30m from the left bank and 95m from the right. At the instant of breaking of the dam, water is released through the breach, forming a positive wave (bore) propagating downstream and a negative wave (rarefaction) spreading upstream. The results for $h_d = 5m$ and after $t = 0.72s$

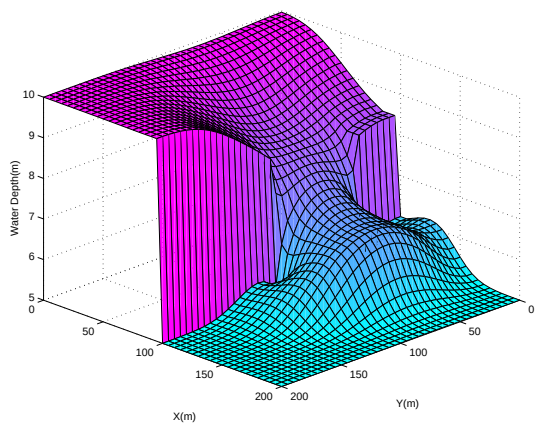

Fig. 1. Water depth for the partial dam-break flow ($h_d = 5m$) at $t = 0.72s$ computed with the upwind relaxation scheme.

are shown in Figs 1, 2, and 3 in terms of water depth, contour of depth and velocity field. The computational parameters used were $\epsilon = 1.E-6$ and $c_1 = 10, c_2 = 6, c_3 = 11, d_1 = 10, d_2 = 5, d_3 = 11$. The difference between the first order upwind scheme and the MUSCL can be clearly seen. The SB limiter has been shown (see Fig. 3) to exhibit sharper resolution of discontinuities, since

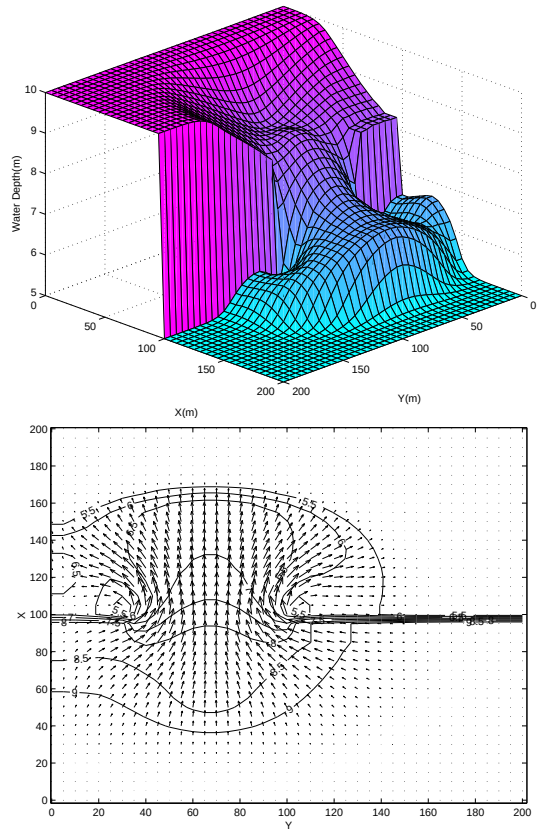

Fig. 2. Water depth and Depth contours with velocity field for the partial dam-break flow ($h_d = 5m$) at $t = 0.72s$ computed with the MUSCL relaxation scheme (MM limiter).

it does not reduce the slope as severely as MM near a discontinuity.

In Fig. 4 the results for $h_d = 0.1m$ are presented using the VL limiter. When there is a finite water depth downstream, a shock front always exists. This is not the case for the dry bed case. In the dry bed case the bore propagates much faster and at time $t = 7.2s$ has reached the boundary of the computational domain boundary. There is also a significant difference in the velocity vector field in the two cases. In the wet bed cases although there is a finite water depth downstream the flow

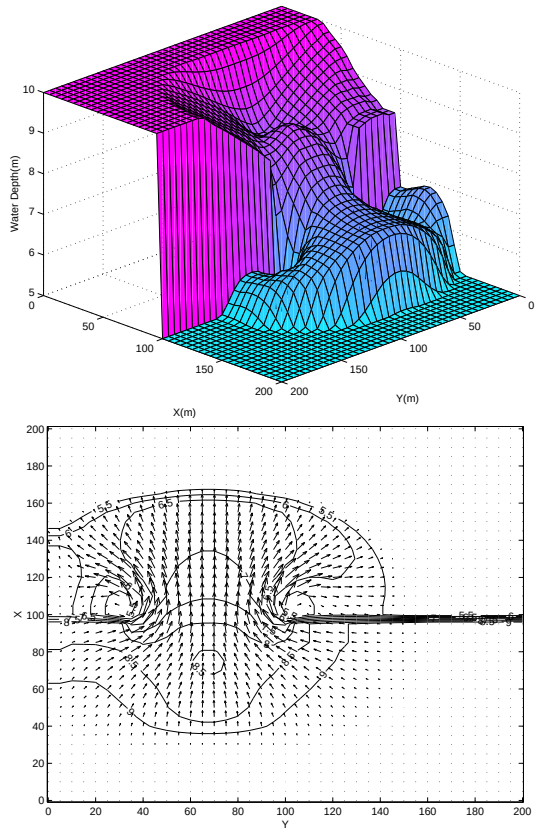

Fig. 3. Water depth and Depth contours with velocity field for the partial dam-break flow ($h_d = 5m$) at $t = 0.72s$ computed with the MUSCL relaxation scheme (SB limiter).

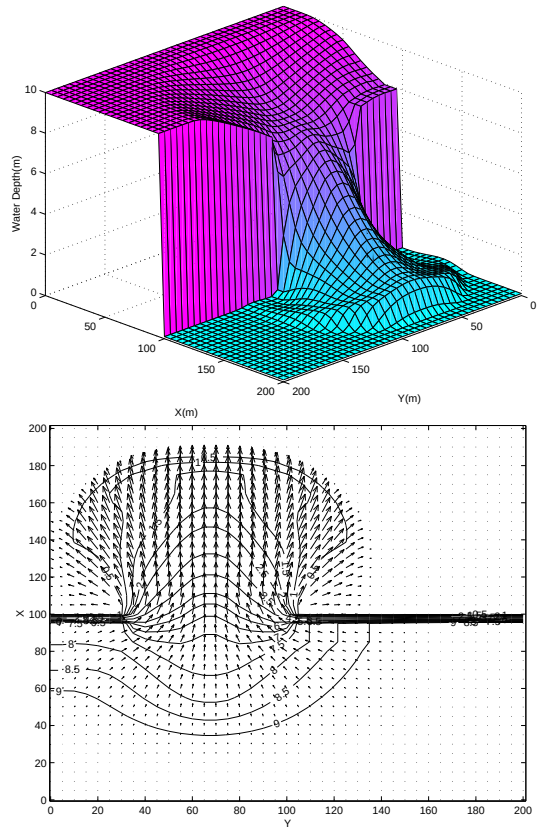

Fig. 4. Water depth and Depth contours with velocity field for the partial dam-break flo w ($h_d = 0.1m$) at $t = 0.72s$ compute ed with the MUSCL relaxation scheme (VL limiter and $c_1 = c_2 = 12, c_3 = 15, d_1 = d_3 = 12, d_2 = 6$).

velocity vanishes. In the dry case, the water depth is extremely small. In the numerical scheme, h and q are the calculated variables. Machine precision will produce finite values for the dependent variable u, calculated as $u = q/h$, even though to machine precision h is considered as zero. These results can be seen in Fig. 5 for a 81×81 square grid. All the results presented here are very similar to others found in the literature, see for example [1],[12]

B. *Circular 2D Dam-Break*

Another typical example is based on the hypothetical test case presented in [1]. It involves the breaking of a circular dam, and it is an important test example for the analysis and performance of the presented algorithms when solving complex shallow flow problems. Initially, the physical model is that of two regions of still water separated by a cylindrical wall (with radius 11m) centered in a $50 \times 50m$ square domain. The water depth within the cylinder is $10m$ and $1m$ outside. The wall is then assumed to be removed completely and no slope or friction is considered, then the circular dam-break waves (rarefaction waves) will spread and propagate radially and symmetrically as the

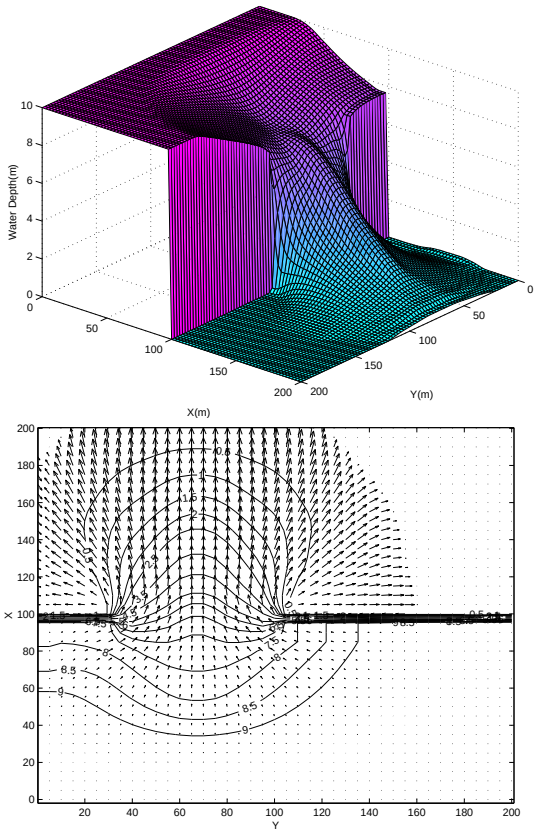

Fig. 5. Depth contours and velocity field for the partial dam-break flow ($h_d = 0m$) at $t = 0.72s$ computed with the MUSCL relaxation scheme (VL limiter and $c_1 = c_2 = 12, c_3 = 15, d_1 = d_3 = 12, d_2 = 10$).

water drains from the deepest region and there is a transition from subcritical to supercritical flow. The results after $t = 0.69s$ are shown in Figs 6, 7, again in terms of water depth, contour of depth and velocity field. The computational parameters used were $\epsilon = 1.E-6$ and $c_1 = c_3 = 12, c_2 = 7, d_1 = d_3 = 12, d_2 = 7$. It can be clearly seen that the waves spread uniformly and symmetrically, with the radial symmetry slightly distorted by the effects of the grid due to the inability to represent a circle on a square grid, but otherwise the solution is very accurate and agrees quite well with those presented in [1], [12] and other works.

The case of an initially dry bed outside the cylinder is also considered here and the results are presented in Fig. 8 It can be seen that no bore forms, instead a rarefaction wave extends into the dry region. The scheme is capable of handling the dry bed problem. The computational parameters used for this case were $\epsilon = 1.E-6$ and $c_1 = c_3 = 12.5, c_2 = 10, d_1 = d_3 = 12.5, d_2 = 10$.

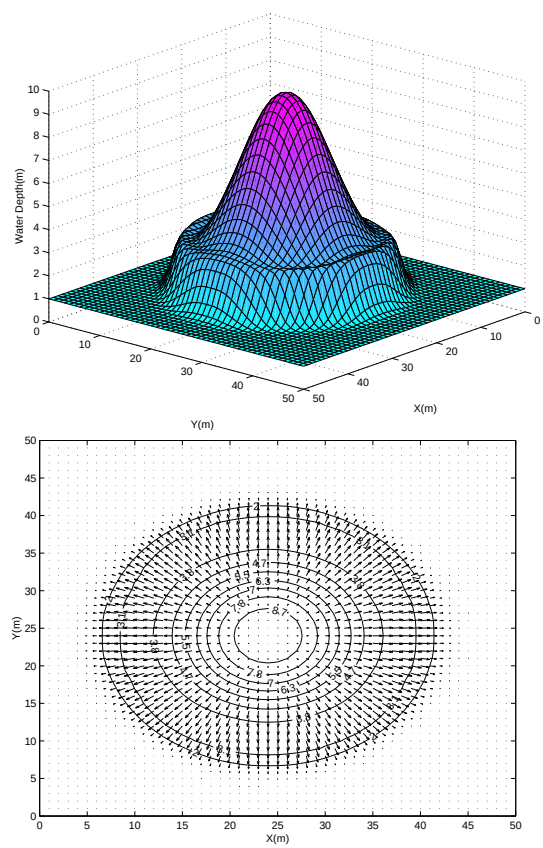

Fig. 6. Water depth and Depth contours with velocity field at $t = 0.69s$ for the circular dam-break flow computed with the upwind relaxation scheme

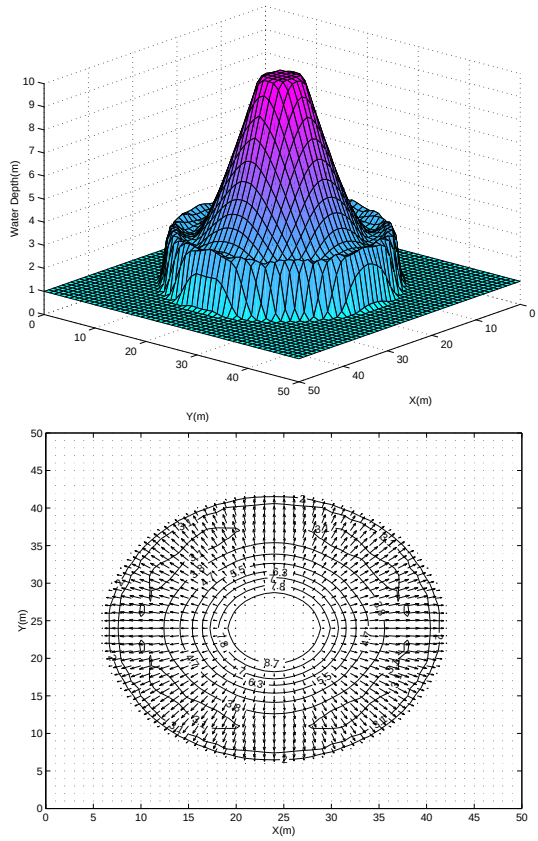

Fig. 7. Depth contours and velocity field at $t = 0.69s$ for the circular dam-break flow computed with the MUSCL relaxation scheme and the SB limiter

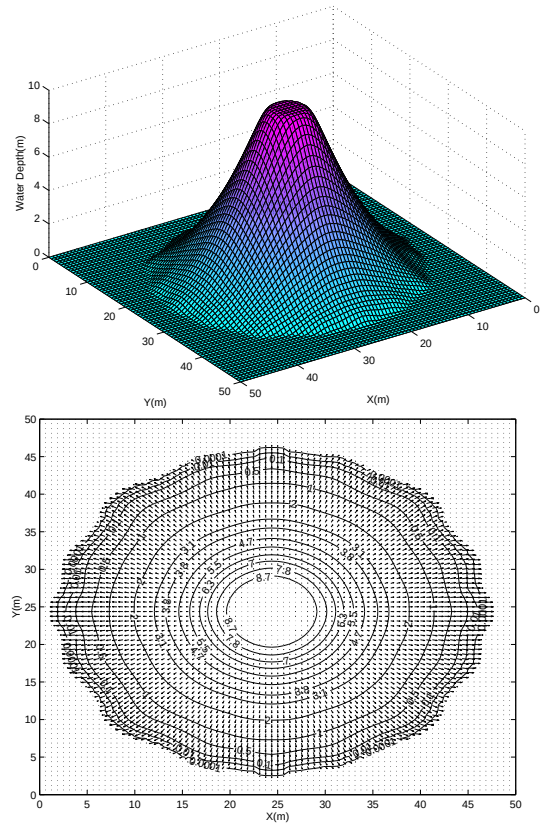

Fig. 8. Depth contours and velocity field at $t = 0.69s$ for the dry bed circular dam-break flow computed with the MUSCL relaxation scheme and the VL limiter

C. Steady flow over a hump

As a problem with a source term present we consider the academic test case of a 1m $\times$ 1m square pool with a symmetric bump situated at the center presented in [2]. The pool is assume totally closed by solid vertical walls. The bump is mathematically defined by

$$Z = \max\left[0, \frac{1}{4} - 5 \quad x - \frac{1}{2} \quad ^{2} + \quad y - \frac{1}{2} \quad ^{2}\Big)\right].$$

Initial conditions covering totally the bump are $h + Z = 0.5m, u_1 = u_2 = 0m/s$. The flow evolves during 60s and the initial steady state must be preserved. The results for scheme (3b) (that was proven in [4] more accurate for similar 1D problems when compared to scheme (3a)) are presented in Fig. 9. A uniform 51×51grid was used and the computational parameters were $\epsilon = 1.E-8$ and $c_1 = c_3 = 2.5, c_2 = 0.5, d_1 = d_3 = 2.5, d_2 = 0.5$. The steady state is correctly maintained, with a small distortion at the point where the bump geometry is discontinuous my construction. The overall equilibrium is conserved with no unphysical velocities appearing in the results that would alter the steady state.

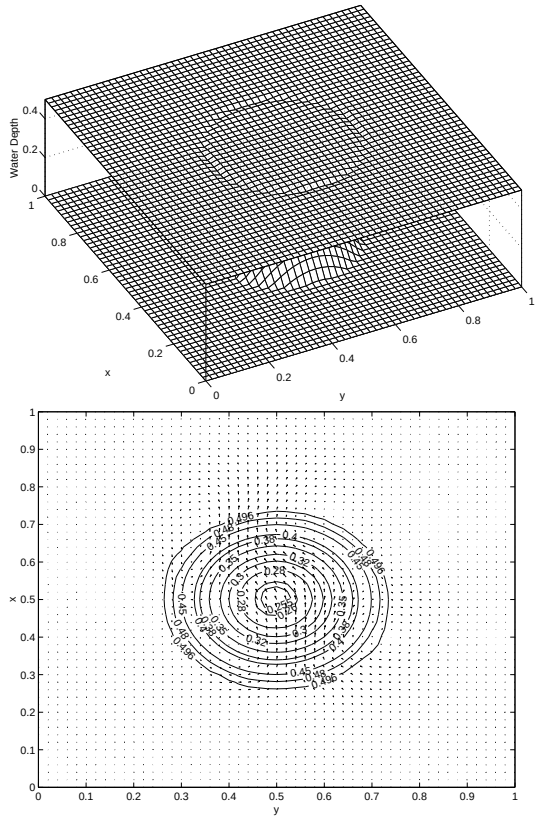

Fig. 9. Water depth over a bump and depth contours with velocity field, for a steady flow over a bump

VI. Conclusions

In the present work a generalization of relaxation schemes have been presented in order to compute shallow water flows in 2D with and without a topography source term present. The main feature of the schemes is their simplicity and robustness. Finite volume shock capturing spatial discretizations, that are Riemann solver free, have been used providing accurate shock resolution. A new way to incorporate the topography source term in 2D was applied with the relaxation model and only small errors were introduced while preserving steady states. The results also demonstrate that relaxation schemes are accurate, simple, efficient and robust and can be of practical consideration.

References

[1] Alcrudo F, Garcia-Navarro P. A high resolution Godunov-type scheme in finite volumes for the 2D shallow water equations. *Int. J. Numer. Meth. Fluids* 19933; **16**:489-505.

[2] Brufau P, Garcia-Navarro P. Unsteady free surface flow simulation over complex topography with a multidimensional upwind technique. *J. Comp. Phys.* 2003;**186**:503-526.

[3] Chalabi A. Convergence of relaxation schemes for hyperbolic conservation laws with stiff source terms. *Math. Comput.* 1999; **68**:955–970.

[4] Delis AI, Katsaounis Th. Relaxation schemes for the shallow water equations. *Int. J. Numer. Meth. Fluids* 2003; **41**:695-719.

[5] Fennema RJ, Chaudhry. Explicit methods for 2D transient free surface flows, *J. Hydraul. Eng. ASCE* 1990; **116**:1013-1034.

[6] Jin S, Xin Z. The relaxing schemes of conservations laws in arbitrary space dimensions. *Comm. Pure Appl. Math.* 1995; **48**:235–277.

[7] Katsoulakis M, Kossioris G, Makridakis Ch. Convergence and error estimates of relaxation schemes for multidimensional conservation laws. *Comm. Partial Differential Equations* 1999; **24**: 395–424.

[8] Lattanzio C, Serre D. Convergence of a relaxation scheme for hyperbolic systems of conservation laws. *Numer. Math.* 2001; **88**:121–134.

[9] Liu TP. Hyperbolic conservation laws with relaxation. *Comm. Math. Phys.* 1987; **108**:153-175.

[10] Natalini R. Convergence to equilibrium for the relaxation approximations of conservation laws. *Comm. Pure Appl. Math.* 1996; **49**:795–823.

[11] Toro EF. Shock-capturing methods for free-surface shallow flows, Wiley, 2001

[12] Zoppou C, Roberts S. Numerical solution of the two-dimensional unsteady dam break. *Applied mathematical Modelling* 2000; **24**:457-475.